

## STRUCTURAL BIOLOGY

# Structure of the cold- and menthol-sensing ion channel TRPM8

Ying Yin,<sup>1\*</sup> Mengyu Wu,<sup>2\*</sup> Lejla Zubcevic,<sup>1</sup> William F. Borschel,<sup>1</sup> Gabriel C. Lander,<sup>2†</sup> Seok-Yong Lee<sup>1†</sup>

Transient receptor potential melastatin (TRPM) cation channels are polymodal sensors that are involved in a variety of physiological processes. Within the TRPM family, member 8 (TRPM8) is the primary cold and menthol sensor in humans. We determined the cryo-electron microscopy structure of the full-length TRPM8 from the collared flycatcher at an overall resolution of ~4.1 Å. Our TRPM8 structure reveals a three-layered architecture. The amino-terminal domain with a fold distinct among known TRP structures, together with the carboxyl-terminal region, forms a large two-layered cytosolic ring that extensively interacts with the transmembrane channel layer. The structure suggests that the menthol-binding site is located within the voltage-sensor-like domain and thus provides a structural glimpse of the design principle of the molecular transducer for cold and menthol sensation.

The transient receptor potential melastatin (TRPM) family, part of the TRP protein superfamily, is composed of eight members, TRPM1 to TRPM8, and is involved in various processes including temperature sensing, ion homeostasis, and redox sensing (1, 2). The TRPM8 channel cDNA was cloned and characterized as the long-sought-after cold and menthol sensor (3, 4). Studies of TRPM8-deficient mice showed that the channel is required for environmental cold sensing (5–7) and that it is the principal mediator of menthol-induced analgesia of acute and inflammatory pain (8). Therefore, TRPM8 is a therapeutic target for treatment of cold-related pain, chronic pain, and migraine (9, 10).

In addition to cold and menthol, TRPM8 is sensitive to voltage and phosphatidylinositol-4,5-bisphosphate (PIP<sub>2</sub>) (11, 12). The molecular landscape of channel sensitization is shaped by the interplay between these four factors, suggesting that TRPM8 is a polymodal sensor that can integrate multiple chemical and physical stimuli into cellular signaling (11, 13). Several thermodynamic models have been put forth to address the mechanism of polymodal sensing by TRPM8 (14–16), but mechanistic understanding of polymodal sensing by TRPM8 remains limited.

All members of the TRPM family contain a large N-terminal region (~700 amino acids) that comprises four regions of high homology (melastatin homology regions, MHRs) (1). These MHR domains appear to be important for channel assembly and trafficking, but their functional roles are not known (17). TRPM8 was also predicted to contain a putative C-terminal coiled coil that is

important for channel assembly, trafficking, and function (17, 18).

Extensive electrophysiological and biochemical studies have identified residues involved in ligand binding, and homology models have attempted to provide a structural context for their locations (19–22). However, in the absence of a structure, these predictions were speculative, and the mechanism of menthol-dependent TRPM8 gating remained unclear.

We conducted structural studies of full-length TRPM8 from the collared flycatcher *Ficedula albicollis* (TRPM8<sub>FA</sub>) using cryo-electron microscopy (cryo-EM). TRPM8<sub>FA</sub> is highly homologous to human and chicken TRPM8 (83 and 94% sequence identity, respectively; fig. S1), which are cold- and menthol-sensitive (14, 20). To prevent proteolysis, we introduced three mutations into TRPM8<sub>FA</sub> (Phe<sup>535</sup>→Ala, Tyr<sup>538</sup>→Asp, and Tyr<sup>539</sup>→Asp). When expressed in human embryonic kidney 293 (HEK293) cells, both the wild-type and the mutant channels exhibited similar menthol-evoked currents and calcium influx, indicating that the mutations do not appreciably affect TRPM8<sub>FA</sub> function (fig. S2). Notably, the half-maximal effective concentration value and the current-voltage relationship of TRPM8<sub>FA</sub> for menthol are comparable to those of human and chicken TRPM8 (14, 20).

TRPM8<sub>FA</sub> was frozen in vitreous ice and imaged using a Titan Krios transmission electron microscope with a K2 Summit direct electron detector (see Methods and fig. S3). The final three-dimensional (3D) reconstruction was resolved to an overall resolution of ~4.1 Å, with local resolutions ranging from ~3.8 Å at the core to ~8 Å at the periphery (Fig. 1 and fig. S3). The quality of the map allowed for de novo model building (see materials and methods) of 75% of the TRPM8<sub>FA</sub> polypeptide (fig. S4 and table S1). The final model for TRPM8<sub>FA</sub> contains amino acids 122 to 1100 with multiple loops missing. Several regions (three β strands in MHRs, C-terminal domain

helix 1, and the C-terminal coiled coil) are built as polyalanine (see materials and methods).

The TRPM8<sub>FA</sub> homotetramer is shaped like a three-layered stack of tetragonal bricks with dimensions of approximately 110 Å by 110 Å by 125 Å (Fig. 1, A and B). The top layer comprises the transmembrane channel domain (TMD) and the lower two layers comprise the cytosolic domain (CD). Each protomer contains a large N-terminal region consisting of MHR1 to 4, a transmembrane channel region, and a C-terminal region (Fig. 1, C and D).

The TMs of TRPM8<sub>FA</sub> assume a fold similar to that of TRPV1 and TRPV2, with a voltage-sensor-like domain (VSLD) made up of transmembrane helical segments S1 to S4, a pore domain formed by S5 and S6 helices, and one pore helix (23, 24) (Figs. 1 and 2). Similar to previously determined TRPV structures, the TRPM8<sub>FA</sub> TMD exhibits a domain-swapped arrangement, with the VSLD of one protomer interacting with the pore domain of the neighboring protomer. However, the TMD of TRPM8<sub>FA</sub> has three features that are distinct from other TRP ion channel architectures. First, relative to the structure of apo TRPV1, the pore helix of TRPM8<sub>FA</sub> is positioned ~12 Å farther away from the central axis, tilted by ~8°, and translated toward the extracellular side by ~5 Å (Fig. 2, A and B). The putative selectivity filter is poorly resolved in the cryo-EM density map, which prevented accurate model building in this region (fig. S5). Sequence comparison with TRPV1 shows that TRPM8 lacks the turret connecting S5 and the pore helix, instead containing a much longer pore loop (fig. S5). Given the differences in the pore helix position and the sequence surrounding the selectivity filter, we speculate that the TRPM8 selectivity filter adopts an organization that is distinct from that of TRPV1. The second distinguishing feature of TRPM8<sub>FA</sub> is the absence of non-α-helical elements (e.g., 3<sub>10</sub> or π helices) in its TMs, which in other TRP channels were proposed to provide helical bending points important for channel gating (23, 25). In TRPM8<sub>FA</sub>, a straight α-helical S4 is connected to α-helical S5 via a sharp turn induced by a conserved proline residue (Fig. 2, C to E). The lack of a bending point in S5 calls into question whether TRPM8<sub>FA</sub> possesses an S4-S5 linker, which is the structural element critical for vanilloid-dependent TRPV1 gating (26); however, it is possible that a transition from α to π helix in the TRPM8<sub>FA</sub> S5 may occur during gating, as was suggested for TRPV2 (23). Despite the absence of an obvious S4-S5 linker, TRPM8<sub>FA</sub> nonetheless forms a domain-swapped tetramer, which is in stark contrast to the calcium-activated K<sup>+</sup> channel Slo1, where a similarly short S4-S5 linker prevents formation of a domain-swapped tetramer (27). The overlay of TRPM8<sub>FA</sub> and TRPV1 protomers reveals that the C-terminal part of TRPM8<sub>FA</sub> S4 is longer and straight such that it can connect with S5 to achieve a domain-swapped configuration. Furthermore, the sharp turn that connects the α-helical S4 and S5 results in a tilt of S5, giving rise to the distinct position of the pore helix as compared to TRPV1 (Fig. 2, B and C). Third,

<sup>1</sup>Department of Biochemistry, Duke University School of Medicine, Durham, NC 27710, USA. <sup>2</sup>Department of Integrative Structural and Computational Biology, The Scripps Research Institute, La Jolla, CA 92037, USA.

\*These authors contributed equally to this work.

†Corresponding author. Email: seok-yong.lee@duke.edu (S.-Y.L.); glander@scripps.edu (G.C.L.)

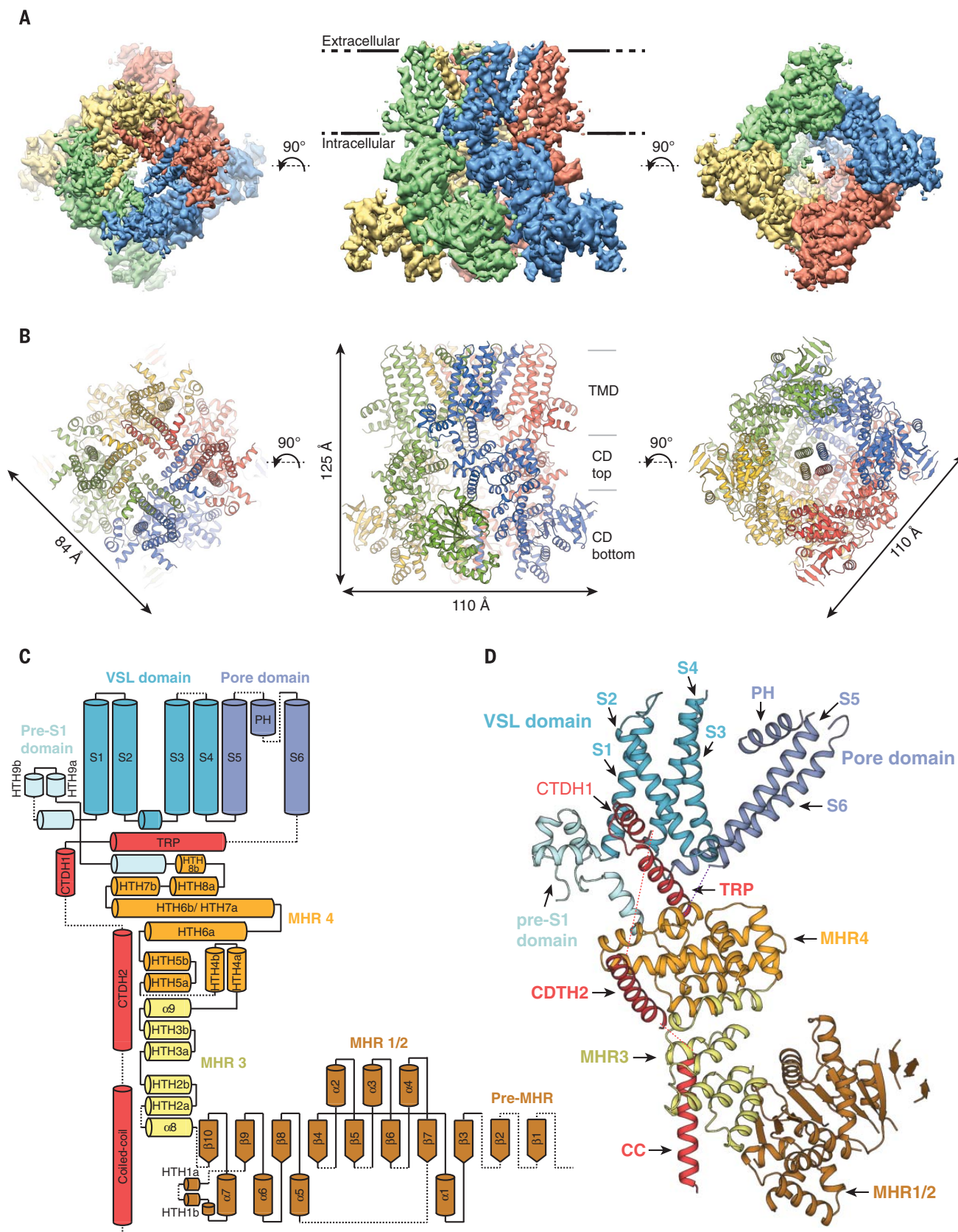


**Fig. 1. Overall architecture of TRPM8.** (A) Cryo-EM reconstruction and (B) model of TRPM8 viewed from the extracellular side (left), from the membrane plane (middle), and from the cytosolic side (right). (C) Topology diagram delineating the protein domains with secondary structure elements. (D) Detailed view of the atomic model of the TRPM8 protomer.

whereas TRPV channels have a cytosolic pre-S1 helix, TRPM8<sub>FA</sub> contains three additional helices between S1 and the cytosolic pre-S1 helix in the putative membrane region: a helix-turn-helix (HTH) followed by an interfacial helix that con-

nects to S1. We term this structural motif, including the cytosolic pre-S1 helix, the “pre-S1 domain.”

The C-terminal portions of the four  $\alpha$ -helical S6s are in proximity of each other, providing a constriction point termed the S6 gate (Fig. 2G

and fig. S5). The Leu<sup>973</sup> residues on each protomer form a tight constriction, with diagonally opposing residues distanced 5.3 Å apart, suggesting that our structure represents a nonconductive conformation (Fig. 2, G, H, and I).

The cytoplasmic domain (CD) is composed of the N-terminal domain (NTD) and the C-terminal domain (CTD) (Fig. 3A). The NTD is composed of four MHRs (MHR1 to MHR4). MHR1 and MHR2, along with a part of the pre-MHR region, form a single domain (MHR1/2) with an  $\alpha/\beta$  fold (Fig. 3D). Unlike a typical  $\alpha/\beta$  fold of five  $\beta$  strands surrounded by  $\alpha$  helices, MHR1/2 contains a large parallel  $\beta$  sheet composed of about 10  $\beta$  strands sandwiched by about four  $\alpha$  helices on each side. The pre-MHR and the tip of MHR1/2 are not well resolved in the reconstruction, precluding model building around this region (Fig. 3 and fig. S4). MHR3 and MHR4 are mostly made up of helix-turn-helix (HTH) motifs, but unlike the ankyrin repeats in TRPV channels, the HTHs in MHR3 and MHR4 do not contain hairpin-like protruding loops. The HTHs within MHR3 stack in a sequential fashion, giving rise to the angled position of MHR1/2 relative to MHR4, and resulting in the L-shape of the protomer (Figs. 1D and 3, A and C). The MHR4 domain, located below the VSLD, consists of five (HTH4 to HTH8) non-sequentially stacked HTH motifs (Fig. 3B). The CTD is composed of three helices that are located C-terminal to the TRP domain (Fig. 3A). The first CTD helix (CTDH1) extends from the TRP domain. It then connects to the second CTD helix (CTDH2) via a long loop, which is positioned below HTH6 and HTH7 of MHR4, and runs almost parallel with the TRP domain (Fig. 3, A and B). The C-terminal region of the CTDH2 points toward the cytoplasmic cavity and connects to a tetrameric coiled coil (CC) at the central axis (Fig. 3, A and B). The limited resolution of the cryo-EM density around the CC prevents accurate modeling of this region, but the relatively short (~25 amino acids) and parallel architecture of the TRPM8<sub>FA</sub> CC contrasts with the long (>50 amino acids), antiparallel architecture observed in the CC fragment structure of TRPM7 (28).

In contrast to TRPV1, TRPM8<sub>FA</sub> makes extensive intra- and intersubunit interactions (Fig. 3E). First, while the interaction between the TMD and CD is primarily mediated by the interfacial TRP domain in TRPV1, in TRPM8<sub>FA</sub> the pre-S1 domain establishes additional TMD-CD interactions through contacts with the tip of HTH7b in MHR4 from the adjacent subunit (Fig. 3F and fig. S6, A and B). Second, the CTDH2 runs parallel to the TRP domain but is translated ~29 Å toward the cytosolic side (Fig. 3G), positioned beneath MHR4 and contacting the MHR1/2 of the adjacent subunit (Fig. 3G and fig. S6, C and D). The CTDH2 is therefore in contact with both the top and the bottom layers of the cytoplasmic ring. Based on its position at this interlayer and intersubunit nexus, the CTDH2 might have a role in channel gating as well as cytoplasmic ring assembly. Third, in the bottom layer of the cytoplasmic ring, the tips of two HTH motifs (HTH2a and HTH2b) from MHR3 and the loop of MHR1/2 from the

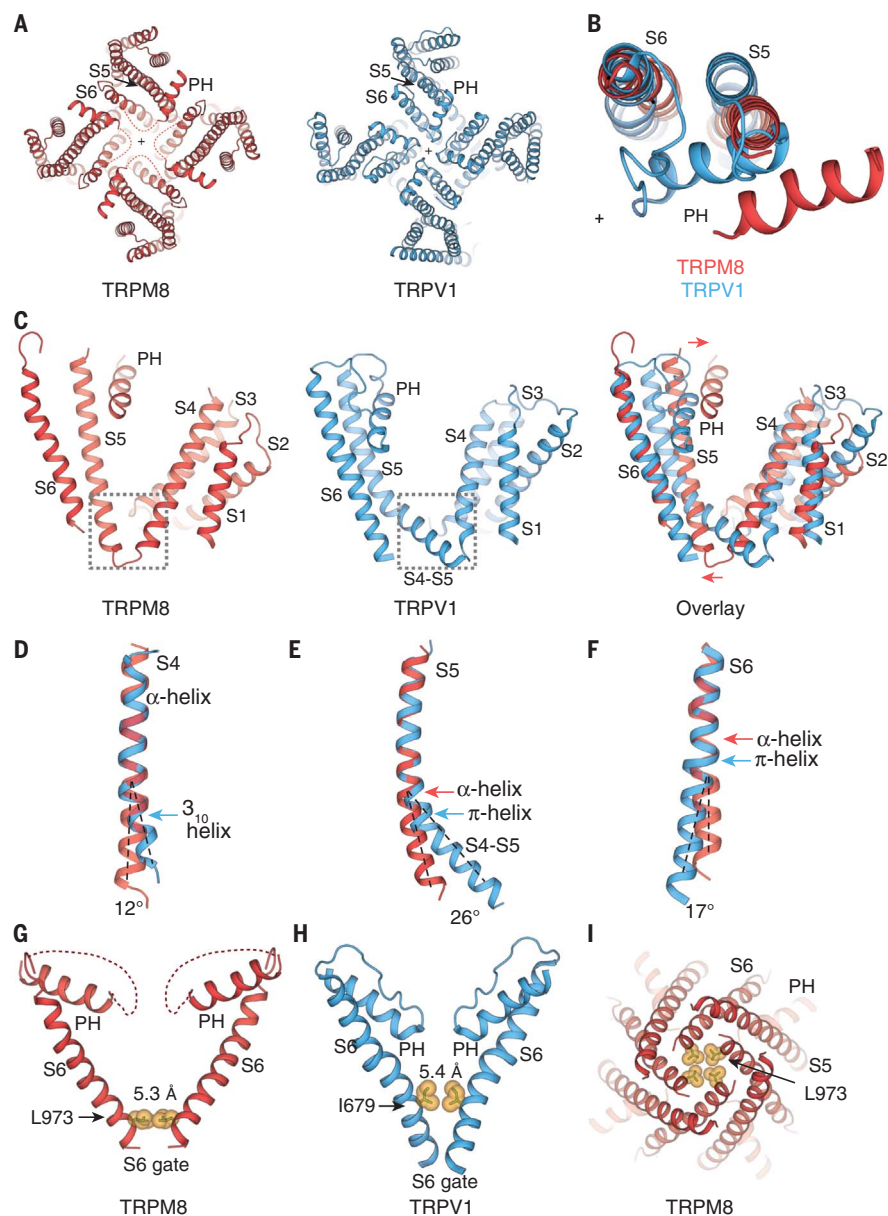


**Fig. 2. Comparison of the transmembrane domain in TRPM8 and TRPV1.** (A) View down the channel pore from the extracellular side. Dashed red lines indicate the selectivity filter and the pore loop linking the pore helix (PH) and S6 in TRPM8, which were not built in the structure owing to the lack of well-resolved cryo-EM density in this region (see fig. S5B). In all panels, the “+” indicates the center of the fourfold symmetry axis. (B) Overlay of the pore domains of TRPM8 (red) and the apo TRPV1 (blue) (PDB ID: 3J5P). The pore helix in TRPM8 is located farther away from the ion permeation pathway. (C) Comparison of the junction between S4 and S5. In TRPM8, S5 is straight and fully  $\alpha$ -helical, and connected to S4 via a sharp turn, while an S4-S5 linker is identified in TRPV1. The overlay illustrates the differing arrangement of the domain swap between TRPM8 and TRPV1. (D to F) The non- $\alpha$ -helical features in the S4 (D), S5 (E) and S6 (F) of TRPV1 (blue) are absent in those of TRPM8 (red). The differences in tilt of helices originating at helical bending points are indicated with dashed lines. (G and H) Comparison of the pores of the TRPM8 and the apo TRPV1 channels, showing that the S6 gate in TRPM8 is formed by Leu<sup>973</sup>. (I) The S6 gate of the TRPM8 structure viewed from the intracellular side. Leu<sup>973</sup> is shown in sphere representation.

neighboring protomer establish an intersubunit network of interactions (Fig. 3H and fig. S6D). These extensive interfacial interactions are the distinguishing features of TRPM8, which may be important for either cold- or menthol-dependent channel gating.

Unlike TRPV channels, TRPM8 contains arginine residues in S4 of the VSLD (Fig. 4A). Arg<sup>842</sup> in

S4 and Lys<sup>856</sup> in S5 (Arg<sup>841</sup> and Lys<sup>855</sup> in TRPM8<sub>FA</sub>, respectively) contribute to the voltage dependence in human TRPM8 (13). In TRPM8<sub>FA</sub>, many aromatic and aliphatic residues within the VSLD form a large hydrophobic “seal” (Fig. 4A) between the extracellular side and the middle of the membrane. Between this hydrophobic seal and the TRP domain, there is a large cavity we term the VSLD

cavity, which is also present in TRPV channels (23, 26). In the TRPM8<sub>FA</sub> structure, Arg<sup>841</sup> points toward the center of the VSLD cavity, where three acidic residues form a negatively charged cluster. Although we cannot unambiguously assign the interaction pairs between the charged residues, this arrangement is more reminiscent of a canonical voltage sensor than the VSLD of TRPV1 (Fig. 4A) (24, 29). We also observed that Lys<sup>855</sup> is located at the beginning of S5 outside the VSLD, but it is unclear how this residue contributes to voltage sensing. Despite the similarities in the positions of charged residues in the TRPM8<sub>FA</sub> VSLD and the canonical voltage sensor, we postulate that the degree and the type of voltage-sensing motion in TRPM8 are different from those of canonical voltage-gated ion channels owing to the large size of the hydrophobic seal and the small gating charge (~1 e<sub>0</sub>) associated with voltage gating of TRPM8 (13).

Many studies have been conducted to elucidate the mechanism of TRPM8 activation by ligand binding. It has been reported that Arg<sup>842</sup> (Arg<sup>841</sup> in TRPM8<sub>FA</sub>) also affects menthol- and cold-dependent activation of human TRPM8. Based on [<sup>3</sup>H]menthol binding studies, this residue appears to interact with menthol (13). Residues Tyr<sup>745</sup> and Tyr<sup>1005</sup> (Tyr<sup>1004</sup> in TRPM8<sub>FA</sub>) were shown to be involved in menthol binding, but not cold sensing (19). Tyr<sup>745</sup> was also found to be critical for binding of the inhibitor SKF96365 (21), further indicating that this residue is central to ligand-dependent gating in TRPM8. In addition, studies have identified Asn<sup>799</sup>, Asp<sup>802</sup>, and Gly<sup>805</sup> as important for icilin binding (20). It was predicted that these ligand-binding sites were all located at the membrane-facing region of S2–S3 (20–22). We can now place these functional studies in the proper structural context. Notably, residue Tyr<sup>745</sup> is located at the middle of S1, directed toward the center of the VSLD cavity (Fig. 4B). This contrasts with its previously predicted location in the membrane-facing side of S2. Furthermore, all residues implicated in menthol binding (Tyr<sup>745</sup>, Arg<sup>841</sup>, and Tyr<sup>1004</sup>) are located in the VSLD cavity (Fig. 4B). We propose that the VSLD cavity is the binding site for menthol and menthol-like molecules in TRPM8. Notably, the corresponding cavity in TRPV channels has been implicated in lipid binding (23, 26) and modulation of channel gating (23). We propose that menthol binding in the VSLD cavity in TRPM8 might modulate the S6 gate through interactions with the TRP domain.

PIP<sub>2</sub> is necessary for TRPM8 activation, as depletion of PIP<sub>2</sub> has been shown to desensitize the channel (11–13). Furthermore, recent studies have suggested that PIP<sub>2</sub> alone can activate TRPM8 (11–13). Mutagenesis studies identified Lys<sup>995</sup>, Arg<sup>998</sup>, and Arg<sup>1008</sup> (Lys<sup>994</sup>, Arg<sup>997</sup>, and Arg<sup>1007</sup> in TRPM8<sub>FA</sub>) as important for PIP<sub>2</sub>-dependent channel gating (11). All of these residues are located in the TRP domain: Arg<sup>1007</sup> is located on the side of the TRP domain facing the VSLD cavity, and Lys<sup>994</sup> and Arg<sup>997</sup> are located on the side of the TRP domain facing the pre-S1 domain and HTH6 in MHR4 from the neighboring subunit

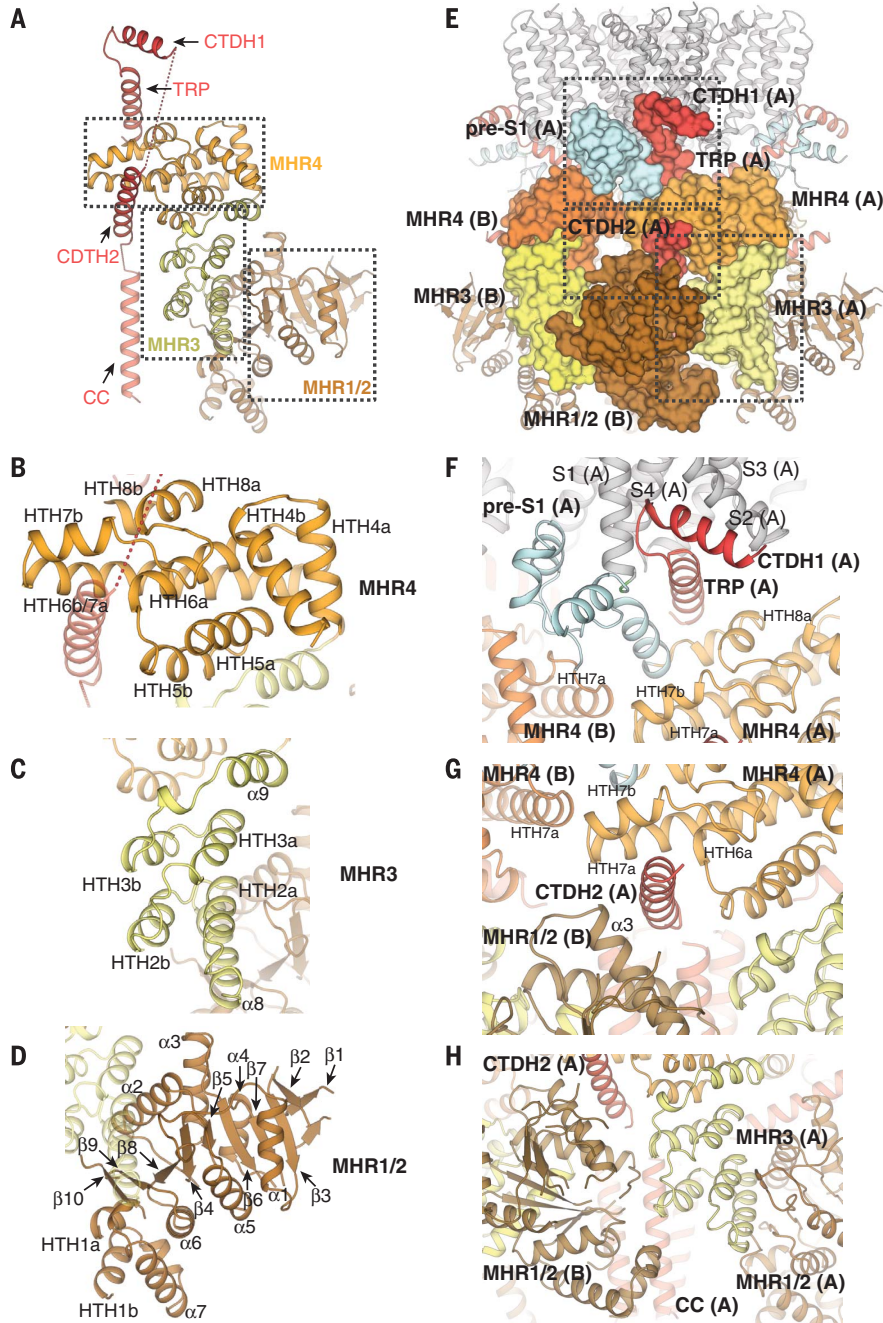


**Fig. 3. The cytoplasmic domain of TRPM8.** (A) The organization of the N- and C-terminal regions of the channel within the cytoplasmic domain (CD). (B to D) Close-up views of MHR4 (B), MHR3 (C), and the single-domain MHR1/2 (D) that comprise the N-terminal domain. (E) Surface representation of the interactions between different domains from the neighboring subunits (A) and (B). (F to H) Close-up views of the domain interfaces that contribute to communication between the TMD and CTD (F), between the top and bottom layers of the cytoplasmic ring (G), and between protomers in the bottom layer of the cytoplasmic ring (H).

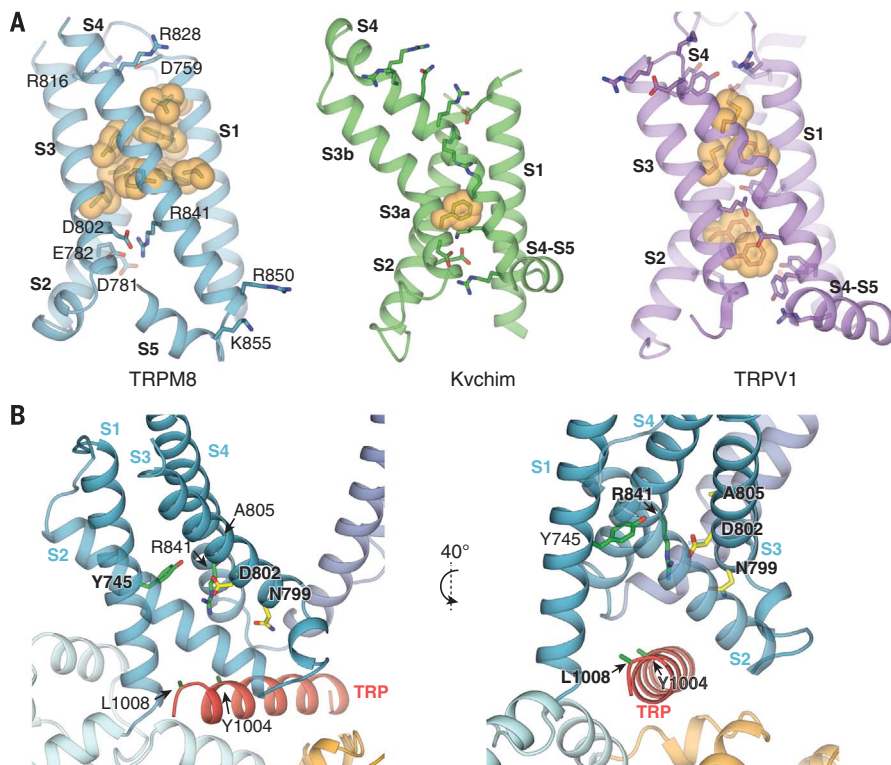


**Fig. 4. The voltage-sensor-like domain (VSLD) and the putative menthol-binding site in the VSLD cavity. (A)** Comparison of the VSLD in TRPM8 (blue) with the canonical voltage-sensor domain in the Kvchim channel (green) (PDB ID: 2R9R) and the VSLD of TRPV1 (purple) (PDB ID: 3J5P). A gating charge Arg<sup>841</sup> in the VSLD of TRPM8 is near three negatively charged amino acids below a large hydrophobic seal (spheres in bright orange) in TRPM8 (left). Many gating charge arginines in S4 of Kvchim are located above and below a small hydrophobic seal (spheres in bright orange) and interact with negatively charged amino acids (middle). The interior of the VSLD of TRPV1 is lined with hydrophobic and polar amino acids. **(B)** Residues critical for the sensitivity of TRPM8 to menthol (shown in green stick representation) were mapped to S1 (Tyr<sup>745</sup>), S4 (Arg<sup>841</sup>), and the TRP domain (Tyr<sup>1004</sup>). Residues implicated in icilin sensitivity of TRPM8 (yellow stick representation) were mapped to S3 (Asn<sup>799</sup> and Asp<sup>802</sup>). All of these residues point toward the VSLD cavity. Single-letter abbreviations for the amino acid residues are as follows: A, Ala; D, Asp; E, Glu; K, Lys; L, Leu; N, Asn; R, Arg; and Y, Tyr.

(fig. S7). Our structure suggests that the VSLD cavity is unlikely to bind PIP<sub>2</sub>, because the net charge of its interior is negative and this cavity is not large enough to accommodate both menthol and PIP<sub>2</sub>. The reported effects of mutations to Arg<sup>1008</sup> may reflect downstream conformational changes following PIP<sub>2</sub> binding. Notably, we found that the interface between the TRP domain, the pre-S1 domain, and MHR4 contains many basic amino acid residues, including the previously identified Lys<sup>994</sup> and Arg<sup>997</sup> (fig. S7). We speculate that PIP<sub>2</sub> binds at this interfacial site, where it could modulate the position of the TRP domain to enable a nondesensitized state. The distinct location of this putative PIP<sub>2</sub> binding site compared to TRPV1 and TRPML reflects the diverse effects of PIP<sub>2</sub> on TRP channels (25, 26).

In the context of previous mutagenesis data, our structural analyses suggest that the ligand-dependent gating mechanism of TRPM8 differs

substantially from TRPV1. In TRPV1, the binding of vanilloid to the S4b and the S4-S5 linker is thought to induce a “swivel” motion in the TRP domain, which would pull on S6 to open the S6 gate (23, 30). We suggest that menthol binds in the VSLD cavity, which is distinct from the vanilloid-binding site in TRPV1. Whereas vanilloid-mediated gating involves non- $\alpha$ -helical elements ( $\beta_{10}$  and  $\pi$  helices) and an S4-S5 linker, neither of these structural features appear to be present in the conformational state of our TRPM8<sub>FA</sub> structure. Thus, we speculate that ligand-induced repositioning of the TRP domain in TRPM8 may directly lead to the opening of the S6 gate.

Our observation of the extensive intersubunit interactions between the TMD and the top layer of the CD ring leads us to speculate that the gating-related TRP domain motion may also involve the top layer of the CD ring (Fig. 3F and fig. S6B). Furthermore, the CTDH2, with its cen-

tral position within the CD and its link with the TRP domain, may be important for coupling the movements of the TRP domain to those of the MHR elements and especially MHR4 (Fig. 3G and fig. S6D). In addition, the tetrameric coiled coil located in the bottom layer ring may play a role in regulating the position of CTDH2.

## REFERENCES AND NOTES

1. A. Fleig, R. Penner, *Trends Pharmacol. Sci.* **25**, 633–639 (2004).
2. A. A. Farooqi *et al.*, *Immunogenetics* **63**, 773–787 (2011).
3. D. D. McKemy, W. M. Neuhausser, D. Julius, *Nature* **416**, 52–58 (2002).
4. A. M. Peier *et al.*, *Cell* **108**, 705–715 (2002).
5. D. M. Bautista *et al.*, *Nature* **448**, 204–208 (2007).
6. A. Dhaka *et al.*, *Neuron* **54**, 371–378 (2007).
7. R. W. Colburn *et al.*, *Neuron* **54**, 379–386 (2007).
8. B. Liu *et al.*, *Pain* **154**, 2169–2177 (2013).
9. M. D. Andrews *et al.*, *ACS Med. Chem. Lett.* **6**, 419–424 (2015).
10. A. D. Weyer, S. G. Lehto, *Pharmaceuticals (Basel)* **10**, 37 (2017).
11. T. Rohács, C. M. Lopes, I. Michailidis, D. E. Logothetis, *Nat. Neurosci.* **8**, 626–634 (2005).
12. B. Liu, F. Qin, *J. Neurosci.* **25**, 1674–1681 (2005).
13. T. Voets, G. Owsianik, A. Janssens, K. Talavera, B. Nilius, *Nat. Chem. Biol.* **3**, 174–182 (2007).
14. T. Voets *et al.*, *Nature* **430**, 748–754 (2004).
15. D. Baez, N. Raddatz, G. Ferreira, C. Gonzalez, R. Latorre, *Curr. Top. Membr.* **74**, 51–87 (2014).
16. D. E. Clapham, G. Miller, *Proc. Natl. Acad. Sci. U.S.A.* **108**, 19492–19497 (2011).
17. C. B. Phelps, R. Gaudet, *J. Biol. Chem.* **282**, 36474–36480 (2007).
18. P. R. Tsuruda, D. Julius, D. L. Minor Jr., *Neuron* **51**, 201–212 (2006).
19. M. Bandell *et al.*, *Nat. Neurosci.* **9**, 493–500 (2006).
20. H. H. Chuang, W. M. Neuhausser, D. Julius, *Neuron* **43**, 859–869 (2004).
21. A. Malkia, M. Pertusa, G. Fernández-Ballester, A. Ferrer-Montiel, F. Viana, *Mol. Pain* **5**, 62 (2009).
22. A. Pedretti, C. Marconi, I. Bettinelli, G. Vistoli, *Biochim. Biophys. Acta* **1788**, 973–982 (2009).
23. L. Zubcevic *et al.*, *Nat. Struct. Mol. Biol.* **23**, 180–186 (2016).
24. M. Liao, E. Cao, D. Julius, Y. Cheng, *Nature* **504**, 107–112 (2013).
25. M. Hirschi *et al.*, *Nature* **550**, 411–414 (2017).
26. Y. Gao, E. Cao, D. Julius, Y. Cheng, *Nature* **534**, 347–351 (2016).
27. X. Tao, R. K. Hite, R. MacKinnon, *Nature* **541**, 46–51 (2017).
28. Y. Fujiwara, D. L. Minor Jr., *J. Mol. Biol.* **383**, 854–870 (2008).
29. S. B. Long, X. Tao, E. B. Campbell, R. MacKinnon, *Nature* **450**, 376–382 (2007).
30. E. Cao, M. Liao, Y. Cheng, D. Julius, *Nature* **504**, 113–118 (2013).

## ACKNOWLEDGMENTS

Cryo-EM data were collected at The Scripps Research Institute (TSRI) electron microscopy facility. We thank Y. Zhang and H. Yang (Duke University) for providing access to their calcium imaging apparatus and guidance to calcium imaging experiments. We thank J.-C. Ducom (TSRI High Performance Computing facility) for computational support, B. Anderson for microscope support, and M. Herzik and S. Chowdhury for helpful discussion and training. We thank Z. Johnson for advice on sample freezing. This work was supported by the National Institutes of Health (grants R35NS097241 to S.-Y.L., DP2EB020402 to G.C.L.). G.C.L. is supported as a Searle Scholar and a Pew Scholar. Computational analyses of EM data were performed using shared instrumentation funded by NIH grant S100D021634. The coordinates are deposited in the Protein Data Bank with the PDB ID 6BPQ, and the electron density maps have been deposited in EMD with the ID EMD-7127.

## SUPPLEMENTARY MATERIALS

www.sciencemag.org/content/359/6372/237/suppl/DC1  
Materials and Methods  
Figs. S1 to S7  
Tables S1  
References (31–50)

3 November 2017; accepted 27 November 2017  
Published online 7 December 2017  
10.1126/science.aan4325

## Structure of the cold- and menthol-sensing ion channel TRPM8

Ying Yin, Mengyu Wu, Lejla Zubcevic, William F. Borschel, Gabriel C. Lander and Seok-Yong Lee

*Science* **359** (6372), 237-241.

DOI: 10.1126/science.aan4325 originally published online December 7, 2017

### Architecture of the TRPM subfamily

Transient receptor potential melastatin (TRPM) ion channels constitute the largest TRP subfamily and are involved in many physiological processes. TRPM8 is the primary cold and menthol sensor, and TRPM4 is associated with cardiovascular disorders. Yin *et al.* and Autzen *et al.* shed light on the general architecture of the TRPM subfamily by solving the structures of TRPM8 and TRPM4, respectively (see the Perspective by Bae *et al.*). The three-layered architecture of the TRPM8 channel provides the framework for understanding the mechanisms of cold and menthol sensing. The two distinct closed states of TRPM4, with and without calcium, reveal a calcium-binding site and calcium-binding-induced conformational changes.

*Science*, this issue p. 237, p. 228; see also p. 160

#### ARTICLE TOOLS

<http://science.sciencemag.org/content/359/6372/237>

#### SUPPLEMENTARY MATERIALS

<http://science.sciencemag.org/content/suppl/2017/12/06/science.aan4325.DC1>

#### RELATED CONTENT

<http://science.sciencemag.org/content/sci/359/6372/228.full>  
<http://science.sciencemag.org/content/sci/359/6372/160.full>

#### REFERENCES

This article cites 50 articles, 4 of which you can access for free  
<http://science.sciencemag.org/content/359/6372/237#BIBL>

#### PERMISSIONS

<http://www.sciencemag.org/help/reprints-and-permissions>

Use of this article is subject to the [Terms of Service](#)